Temperature-dependence of oxygen reduction activity on Pt/C and PtCr/C electrocatalysts synthesized from microwave-heated diethylene glycol method

Nihat Ege Sahin [a,b], Teko W. Napporn [a,*], Laetitia Dubau [c], Figen Kadirgan [d], Jean-Michel Léger [a], K. Boniface Kokoh [a]

[a] IC2MP, UMR 7285, CNRS, Université de Poitiers, "Équipe SAMCat", 4, rue Michel Brunet, B27, TSA 51106, 86073 Poitiers cedex 09, France
[b] Department of Nano-Science and Nano-Engineering, Istanbul Technical University, 34469, Maslak, Istanbul,Turkey
[c] Laboratoire d'Electrochimie et de Physico-chimie des Matériaux et des Interfaces LEPMI-Phelma, UMR 5279, CNRS, Grenoble-INP, Université de Savoie, Université Joseph Fourier, BP 75, 38402, Saint Martin d'Hères Cedex, France
[d] Department of Chemistry, Faculty of Science and Letters, Istanbul Technical University, 34469, Maslak, Istanbul, Turkey

ARTICLE INFO

ABSTRACT

This work reports first the synthesis of carbon supported Pt and Pt-Cr electrode materials from microwave-heated diethylene glycol (DEG) without additional protective agents. The prepared electrocatalysts have superior electrochemical activity and stability than those previously reported in acidic medium. Transmission electron microscopy (TEM) characterizations of these materials reveal uniformly dispersed particles with a mean size of *ca.* 1.20 nm. The morphological changes of these two materials were investigated by identical location-transmission electron microscopy (IL-TEM) after classical durability test. The electrocatalytic activity towards the oxygen reduction reaction (ORR) was investigated using rotating disk electrode (RDE) and rotating ring disk electrode (RRDE) techniques in 0.1 mol L^{-1} HClO$_4$. The kinetic parameters were assessed through the Koutecký-Levich equation at 20, 30 and 40 °C. Electrochemical measurements demonstrate that significantly higher catalytic activity was observed on the Pt-Cr/C electrocatalyst than on Pt/C. The RRDE analysis shows that the ORR mainly involves a four-electron reduction mechanism to water with the formation of a very low H$_2$O$_2$ amount as reaction intermediate.

© 2016 Elsevier B.V. All rights reserved.

1. Introduction

With the depletion of fossil fuels, the development of fuel cell technology for producing sustainable energy conversion and storage devices are of great importance. Fuel cells and electrolysis processes utilize, alternative energy sources which have for most of them high energy density and low environmental impacts. The synthesis of advanced, effective and durable electrode materials still remains challenging to pave the way of their growing commercialization in various current smart energy devices and networks. To achieve this goal, the mechanisms of these electrochemical reactions and their related kinetic parameters have been the main research interest in the field of electrocatalysis over several decades [1–5]. The oxygen reduction reaction (ORR) involving a multi-electron transfer is a process remaining a non-elucidated complex reaction in the cathodic compartment of a fuel cell and strongly depending on the nature of the electrode surface. Norskov et al. [6] reported that platinum has the ideal electrocatalyst surface that can selectively activate the molecular oxygen with weakly-required binding oxygen species. Non-noble metals such as 3d transition elements show a synergistic effect on platinum *via* the so-called strain and ligand effect inducing lower adsorption strength of ORR intermediates. Secondary, non-noble metal effectively reduce the density of states (DOS) of the Pt d-band at Fermi level, which prevents formation of surface Pt-oxide. Therefore, alloying platinum with a non-noble transition metal reduces the Pt-O formation and thus improves the ORR activity. Moreover, the activity enhancement of the latter reaction results in an increased d-electron vacancy at the Pt surface layer [2], on the basis of the interplay between a decrease of the electronic Pt d-vacancy [7] and the shortening of the Pt-Pt inter atomic distance by alloying [8]. To identify the mechanistic reaction pathways and to propose

a diagnostic criterion to discriminate between the different pathways for oxygen reduction reaction, several reaction schemes have been proposed in the literature [9–13]. From the thermodynamic data, the Nernst equations (Eqs. (1)–(3)) associated with the oxygen reduction reactions can be deduced. The corresponding equilibrium potentials give 1.229, 0.695, 1.763 V vs. the standard hydrogen electrode (SHE), respectively.

$$E_{O_2/H_2O} = E^o_{O_2/H_2O} - \frac{RT}{4F} \ln \left(\frac{a^2_{H_2O}}{a_{O_2} a^4_{H^+}} \right) (E^o_{O_2/H_2O} = +1.229V) \quad (1)$$

$$E_{O_2/H_2O_2} = E^o_{O_2/H_2O_2} - \frac{RT}{2F} \ln \left(\frac{a_{H_2O_2}}{a_{O_2} a^2_{H^+}} \right) (E^o_{O_2/H_2O_2} = +0.695V) \quad (2)$$

$$E_{H_2O_2/H_2O} = E^o_{H_2O_2/H_2O} - \frac{RT}{2F}$$

$$\ln \left(\frac{a^2_{H_2O}}{a_{H_2O_2} a^2_{H^+}} \right) (E^o_{H_2O_2/H_2O} = +1.763V) \quad (3)$$

where the $E^o_{i/j}$ is defined as standard potential of electrochemical couple i/j (V vs. SHE), R is the ideal gas constant (8.314 J mol^{-1} K^{-1}), T is the absolute temperature (K), F is the Faraday constant (96485 C mol^{-1}) a_i and a_j are the activities of the redox couple i/j [14,15]. As SHE is a virtual reference electrode, potentials of the experimental data are presented in reference hydrogen electrode (RHE) by using Eq. (4).

$$E_{RHE} = E_{SHE} - \frac{RT}{nF} pH \quad (4)$$

As the participation of H_2O_2 in the oxygen reduction reaction is highly undesirable mainly due to the decrease of the current efficiency, the dominant reaction pathway is deeply investigated by different research groups. The oxygen reduction mechanism is investigated by three convenient empirical descriptions: (i) the dissociative, (ii) the associative and (iii) the peroxo mechanism [14,16]. The four-electron reduction pathway [2,17] is well-catalyzed by platinum [18,19] and platinum-based alloy nanoparticles [20–23] in order to accelerate the process and conversion of chemical energy to electrical energy. Electrochemical reactions are defined by a transfer of electric charge of electrons and/or ions through the electrode/electrolyte interface or at the metal/electrolyte boundary. In order to understand the mechanism and the electrochemical reaction kinetics, it is essential to get information about structures of electroreactive molecules at heterogeneous electrode/electrolyte interfaces that contain short-lived intermediates and solvents [24,25]. Hydrodynamic voltammetry techniques using the RDE and RRDE are helpful to get some mechanistic insights on the electrocatalytic reduction of oxygen and the potential dependence of peroxide intermediate formation, respectively.
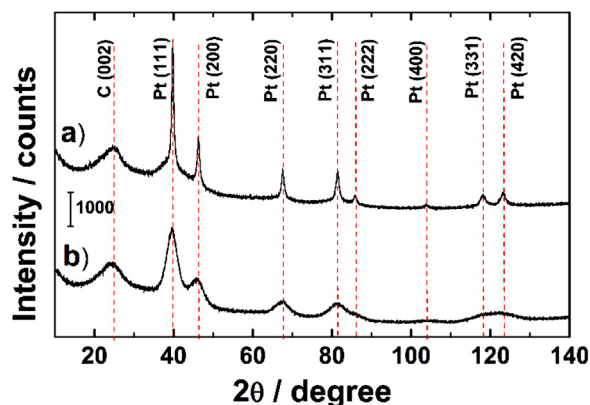
A number of studies reveal that the ORR electrocatalytic activity strongly depends on the composition of nanostructured electrocatalysts [26,27], their morphology [26,28–30], and their particle size [27,31]. It is also well known that the key factor for their synthesis is the nucleation control and the growth rates of the different precursors. In that respect, the polyol method is well-adapted. To get homogeneous and well-dispersed nanoparticles, the optimization of some synthesis parameters including (i) type of polyol solvent [19,32,33]; (ii) salt concentration and pH value [33,34], (iii) microwave power, reaction time, temperature and redox potentials between noble metal and transition metal [35–38], (iv) power density of ultrasonic treatment, [39,40], is needed. In previous works, Pt-based binary [41–46] and ternary [47–49] alloy electrocatalysts were reported to exhibit enhanced ORR activity resulted from their unique synergistic effects. Carbon supported

PtCr materials resulted in different types of preparation were already used as electrocatalysts in investigating the oxygen reduction reaction [21,22,50–52]. Yang et al. [51] investigated the oxygen reduction activity on PtCr/C alloy nanoparticles, prepared via a Pt-carbonyl route. The prepared PtCr/C (1:1) alloy catalyst with a metal loading of 20 wt.% displayed slightly higher catalytic activity when compared to Pt/C (from E-TEK, 20 wt.%) in a 0.5 mol L^{-1} HClO$_4$ electrolyte. The onset potential of alloyed PtCr/C catalysts is higher than that of the Pt/C (E-TEK, 20 wt.%) one, suggesting that the alloy surface is more favored. Additionally, Yang et al. [53] reported that the alloyed PtCr/C nanoparticles with different atomic ratio prepared from the carbonyl synthetic method showed a better activity towards oxygen reduction as compared to the non-alloyed PtCr catalysts [54] prepared by using the Bonnemann colloidal method. Furthermore, the authors reported the significant enhancement factor in both the specific activity (SA) and mass activity (MA) of the alloyed PtCr/C catalysts for oxygen reduction in comparison to Pt/C (E-TEK, 20 wt.%). Jeon et al. [49] reported a comparative study on electrocatalytic reduction of oxygen on Pt$_{30}$Cr$_{70}$/C, Pt$_{30}$Co$_{70}$/C and Pt$_{30}$Co$_{30}$Cr$_{40}$/C alloy catalysts prepared by using NaBH$_4$ reduction method. They noticed a remarkable improvement of oxygen reduction specific activity on these alloyed catalysts in 0.5 mol L^{-1} H$_2$SO$_4$ compared with that of Pt/C. They also observed that when the prepared catalysts were annealed at 900 °C, the oxygen reduction specific activity of the alloy catalysts decreases in the order of PtCo/C > PtCoCr/C > PtCr/C > Pt/C, respectively. Antolini et al. [50] prepared various PtCr/C electrocatalysts by using NaBH$_4$ reduction method with a metal loading of 20 wt.%. They highlighted that the Pt$_3$Cr/C electrocatalyst exhibited the highest catalytic activity towards the ORR with two linear Tafel regions in 1.0 mol L^{-1} H$_2$SO$_4$. The Tafel slopes were evaluated as 52–56 and 120 mV dec^{-1} for low current density and high current density regions, respectively, suggesting that the alloy catalyst possesses the similar oxygen reduction mechanism through the addition of chromium to platinum. The breakthrough of the present purpose concerns the synthesis of uniformly dispersed Pt/C and Pt-Cr/C through microwave-assisted polyol reduction method using diethylene glycol (DEG) as both solvent and reducing agent. DEG is of significant importance due to its molecular structure which provides a better chelate effect, its viscosity which prevents from the agglomeration and its higher boiling point (245 °C) which makes it possible to dissolve inorganic salts and to avoid an excessive bubble formation [37]. The size of these carbon supported Pt and PtCr nanomaterials estimated in the range of 0.6 and 2.20 nm allowed to use them as cathode catalysts. The present study is a comparative investigation of the ORR activity and stability. Furthermore, the temperature dependency of the kinetic parameters such as limiting current density (j$_L$, mA cm^{-2}), intrinsic kinetic current density (j$_k$′, mA cm^{-2}), exchange current density (j$_0$, mA cm^{-2}), Tafel slope (b, mV dec^{-1}), number of transferred electrons, and the assessment of the hydrogen peroxide formation were also considered.

2. Experimental

2.1. Synthesis of Pt/C and PtCr/C electrocatalysts

Pt/C and Pt-Cr/C electrocatalysts were synthesized by a microwave-heated diethylene glycol method characterized by the reduction of Pt (IV) and Cr (III) ions in heated-diethylene glycol solution at a pH value of 12. The synthesis process is briefly described as follows: the required amount of H$_2$PtCl$_6$, 6H$_2$O (Sigma Aldrich ≥ 37.5% metal based) and CrCl$_3$ (Alfa Aesar) precursors were dissolved in 100 mL diethylene glycol through ultrasonication operating at 45 kHz with a maximum power output of 80 W for 4 min. The pH value of the solution was slowly adjusted to 12

Fig. 1. X-ray diffraction patterns of Vulcan XC72 carbon supported Pt (a) and PtCr (b) nanoparticles.

using $1.0\,\mathrm{mol\,L^{-1}}$ NaOH prepared in the DEG solvent. Vulcan XC-72 carbon black was mixed in the solution to facilitate the dispersion of the metal particles and their deposition on this substrate during the reduction step. Afterwards the mixture was stirred at 1000 rpm for 20 min until yielding a homogeneous black suspension that was placed in the microwave oven. The mixture was heated in the microwave oven (MasII) with the power output of 800 W at $150\,^{\circ}\mathrm{C}$ under N_2 gas flowing for 30 min. The pH value was adjusted to 3 and the solution was stirred at 500 rpm for 12 h. Finally, the resulting suspension was centrifuged, washed through 200 mL acetone and 600 mL ultra-pure water and dried in oven at $70\,^{\circ}\mathrm{C}$ for 12 h. The expected metal loading of the prepared electrocatalysts in this work is 30 wt.%.

2.2. Physicochemical characterization

The crystallographic structure and crystallite size of the as-prepared electrocatalysts were conducted by using a PANanalytical X'Pert Pro MDP vertical diffractometer with a copper tube powdered at 40 kV and 40 mA ($\mathrm{Cu,K\alpha 1 = 1.54060\,\AA}$ and $\mathrm{Cu,K\alpha 2 = 1.54443\,\AA}$). To avoid the interference from the kβ component, a nickel filter was installed in a secondary optic. X-ray diffraction pattern was investigated from 10 to 140° in step mode, with 0.07° and fixed acquisition time of 2 min/step. The width of the (220) peak was used to calculate the mean crystallite size and lattice parameters of the nanoparticles according to Scherrer's equation and the Bragg formula, respectively.
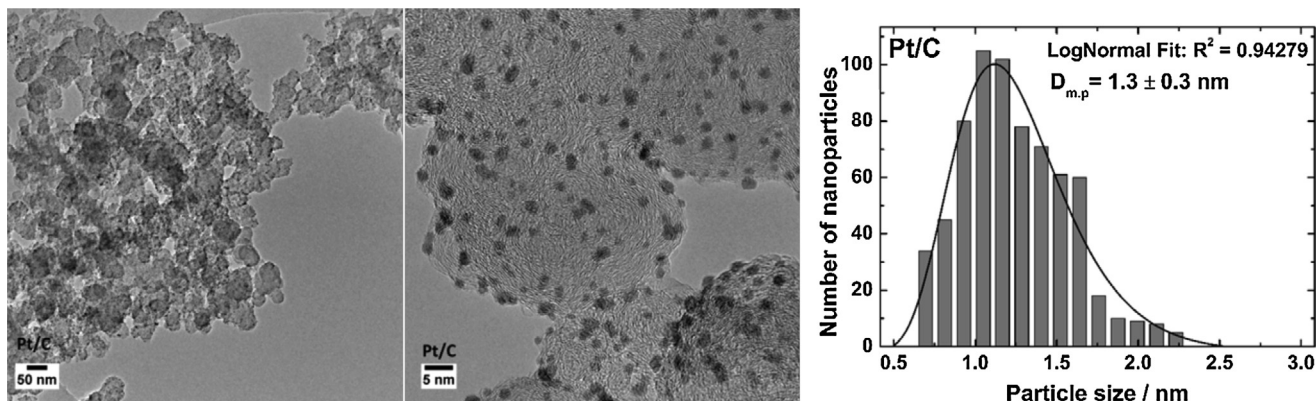
The morphological observation of nanoparticles dispersion on the Vulcan XC-72 carbon support and their size were performed by high-resolution transmission electron microscopy (HRTEM). The

measurements were carried out in a JEOL JEM-2100VRP LaB6 high-resolution transmission electron microscope working at 200 kV accelerating voltage. The point and linear resolutions were 0.19 nm and 0.14 nm, respectively. The TEM Cu grids were prepared by depositing a few drops of a mixture composed of the catalyst powder dispersed in ethanol. The nanoparticle size distribution and the mean particle size were evaluated by ImageJ® free software by measuring the diameter of at least 1000 isolated nanoparticles.

2.3. Electrochemical measurements

Electrochemical experiments were conducted with a rotating disk electrode (RDE, Radiometer Copenhagen EDI101) and a rotating ring disk electrode (RRDE, Pine Instrument) in a thermostated three-electrode electrochemical cell. A Voltalab PGZ 402 (Radiometer analytical) potentiostat and a bipotentiostat (Pine Instrument) were employed for the electrochemical testing. The reference and counter electrodes were saturated calomel electrode (SCE) and a glassy carbon plate (5 cm² geometric surface area), respectively. All potentials were normalized with reversible hydrogen electrode (RHE) scale. To avoid the electrolyte contamination by chloride the reference electrode was separated from the working electrode compartment by a Luggin-Haber ionic bridge.

Prior to electrochemical measurements, the glassy carbon electrode was polished with three different grades of Al_2O_3 slurry $1.0\,\mu m$, $0.5\,\mu m$ and $0.05\,\mu m$ on a synthetic cloth, then rinsed with ultra pure water and ultrasonicated in water and ethanol for 5 min. A homogeneous catalytic ink was prepared with 6.0 mg of catalytic powder, $500\,\mu L$ ultra pure water and a $50\,\mu L$ Nafion® suspension (5 wt.% from Aldrich). This mixture was ultrasonically dispersed for 45 min. The catalytic ink was dropped on the surface of the glassy carbon substrate using a microsyringe and dried under a N_2 gas flow for 5 min. The metal loading deposited onto the disk of RRDE was $102\,\mu g\,cm^{-2}$. For RDE the geometric surface area of the glassy carbon (GC) disk is 0.071 cm², while for RRDE, the disk (GC) and the ring (Pt) have, respectively, 0.196 and 0.110 cm² as geometric surface areas. RRDE measurements were carried out in an aqueous solution containing $0.1\,\mathrm{mol\,L^{-1}}$ $HClO_4$ (70% Merck-Suprapur) as a supporting electrolyte. Herein, ultra pure water was from Milli-Q® Millipore (18.2 MΩ cm at $20\,^{\circ}\mathrm{C}$). Prior to the electrochemical measurements, the working electrode was immersed in oxygen free electrolyte and cycled several times between 0.05 and 1.24 V vs. RHE until reaching a clean electrode surface with a steady-state cyclic voltammogram. The electrochemically active surface area (ECSA) of each electrocatalyst is determined by integrating the charge in the hydrogen adsorption–desorption region between 0.35 and 0.05 V vs. RHE recorded at a scan rate of 20 mV s⁻¹ in N_2-deaerated $0.1\,\mathrm{mol\,L^{-1}}$ $HClO_4$. ORR polarization curves in oxygen

Fig. 2. HRTEM micrographs and their corresponding particle size distribution (histograms were fitted using the log-normal function) of nanostructured Pt/C.
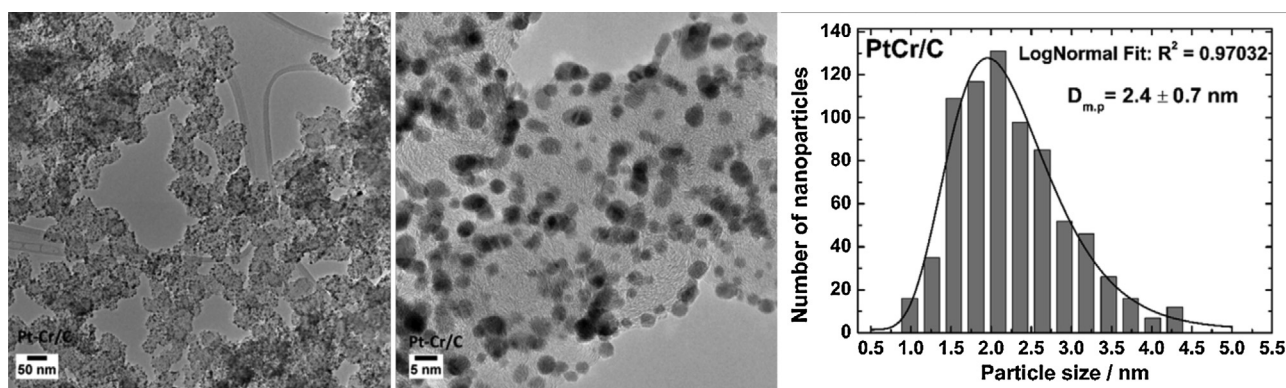
Fig. 3. HRTEM micrographs and their corresponding particle size distribution (histograms were fitted using the log-normal function) of nanostructured Pt-Cr/C.
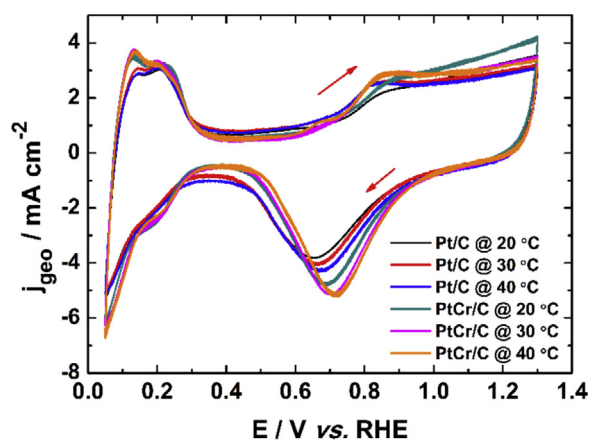

Fig. 4. Cyclic voltammograms of the Pt/C and Pt-Cr/C electrocatalysts in a N_2-deareated $0.1\,mol\,L^{-1}$ $HClO_4$ solution recorded at $50\,mV\,s^{-1}$ and 20, 30, 40 °C.

Table 1
XRD parameters of supported Pt and PtCr nanoparticles for different (hkl) planes.

(hkl) plane	Material	2θ (°)	d_{hkl} (Å)	a_{hkl} (Å)	a_{Bragg} (Å)
(111)	Pt/C	39.79	2.2652	3.9234	3.9235
	PtCr/C	39.47	2.2828	3.9539	3.9539
(200)	Pt/C	46.26	1.9625	3.9250	3.9251
	PtCr/C	46.10	1.9687	3.9374	3.9375
(220)	Pt/C	67.61	1.3856	3.9190	3.9189
	PtCr/C	67.25	1.3922	3.9377	3.9379
(311)	Pt/C	81.36	1.1827	3.9225	3.9226
	PtCr/C	81.15	1.1852	3.9309	3.9309
(222)	Pt/C	86.01	1.1302	3.9151	3.9153
	PtCr/C	85.79	1.1449	3.9660	3.9234
(400)	Pt/C	103.72	0.9802	3.9208	3.9208
	PtCr/C	105.06	0.9819	3.9276	3.8854
(331)	Pt/C	118.04	0.8992	3.9195	3.9195
	PtCr/C	117.97	0.9093	3.9635	3.9209
(420)	Pt/C	123.31	0.8759	3.9171	3.9173
	PtCr/C	122.52	0.8889	3.9752	3.9320

saturated supporting electrolyte were recorded at different rotation rates (400, 900, 1600 and 2500 rpm) and with a scan rate of $5\,mV\,s^{-1}$.

2.4. Stability tests of the electrode materials

Stability tests were performed in $0.1\,mol\,L^{-1}$ $HClO_4$ at 30 °C first by cyclic voltammetry in the potential range 0.05–1.23 V *vs.* RHE to ensure that the characteristic electrochemical response of the Pt/C and Pt-Cr/C catalysts was stable. The electrochemical surface area (ECSA) of the Pt/C and Pt-Cr/C electrocatalysts was determined by CO-stripping measurements. The CO saturation coverage was established by bubbling CO for 6 min and purging to remove free CO with Ar for 39 min, while keeping the electrode potential at $E = 0.1\,V$ *vs.* RHE. It was assumed that the electrooxidation of an adsorbed CO monolayer requires $420\,\mu C$ per cm^2. The Accelerated Stress Tests (AST) investigated in this study consisted of 5000 potential cycles between 0.60 and 1.00 V *vs.* RHE at $v = 50\,mV\,s^{-1}$. Such experimental conditions simulate the typical potential range experienced by a cathode material during PEMFC operation (*i.e.* at high and low current density, during idling and open circuit conditions). At the end of the test, the electrolyte was degassed with Ar and another CO stripping voltammogram was recorded to evaluate the ECSA changes induced by the AST.

The ORR activity was also evaluated before and after the AST. The linear sweep experiments were conducted in O_2-saturated $0.1\,mol\,L^{-1}$ $HClO_4$ solution by sweeping the potential from 0.40 to 1.05 V at a scan rate of $5\,mV\,s^{-1}$ at different rotation rates. The ORR specific/mass activity was determined by normalizing the current measured at $E = 0.90\,V$ *vs.* RHE, after correction from the oxygen
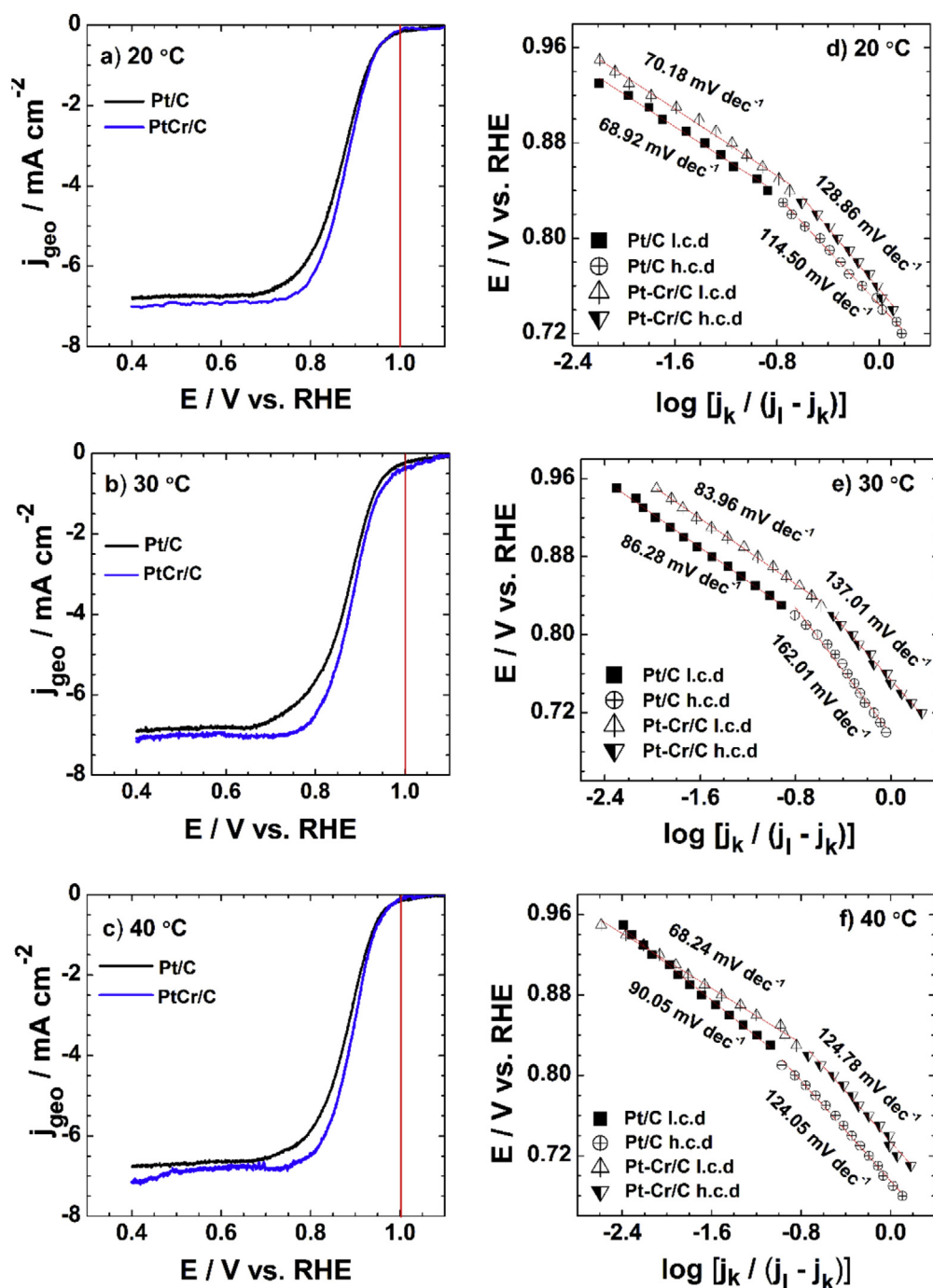
diffusion in the solution and the Ohmic drop, with the real surface area/mass of deposited Pt, respectively.

To unveil the morphological changes of the Pt/C and Pt-Cr/C electrocatalysts, Identical-Location TEM were carried out following the same AST (5000 potential cycles between 0.60 and 1.00 V *vs.* RHE at $v = 50\,mV\,s^{-1}$). The electrocatalysts were deposited onto a gold grid (300 mesh, Lacey Carbon; Agar Sc. UK), and examined with a JEOL 2010 TEM operated at 200 kV with a point-to-point resolution of 0.19 nm. Five randomly selected carbon particles located at different places of the TEM grid were imaged at low (50 k) and high (200 k) magnification. After the AST, the TEM grid was rinsed with MQ-grade water, dried in air, and transferred back for TEM analyses in exactly the same position.

3. Results and discussion

3.1. XRD analysis of Pt/C and PtCr/C electrocatalysts

Fig. 1 displays the X-ray diffraction patterns of the Pt/C and PtCr/C materials that exhibit the same face centered cubic (fcc) crystallographic structure. Note that the peak at *ca.* $2\theta = 25°$ corresponds to graphite (002) crystallographic plane of Vulcan XC-72 carbon. The peaks at 39.8, 46.3, 67.6, 81.3, 86.0, 103.7, 118.0 and 123.3° correspond, respectively to the reflection planes (111), (200), (220), (311), (222), (400), (331) and (420) of the Pt fcc structure. No Pt oxide phase is observed from XRD analysis. Besides, the patterns of Pt-Cr/C nanoparticles exhibit the same fcc crys-
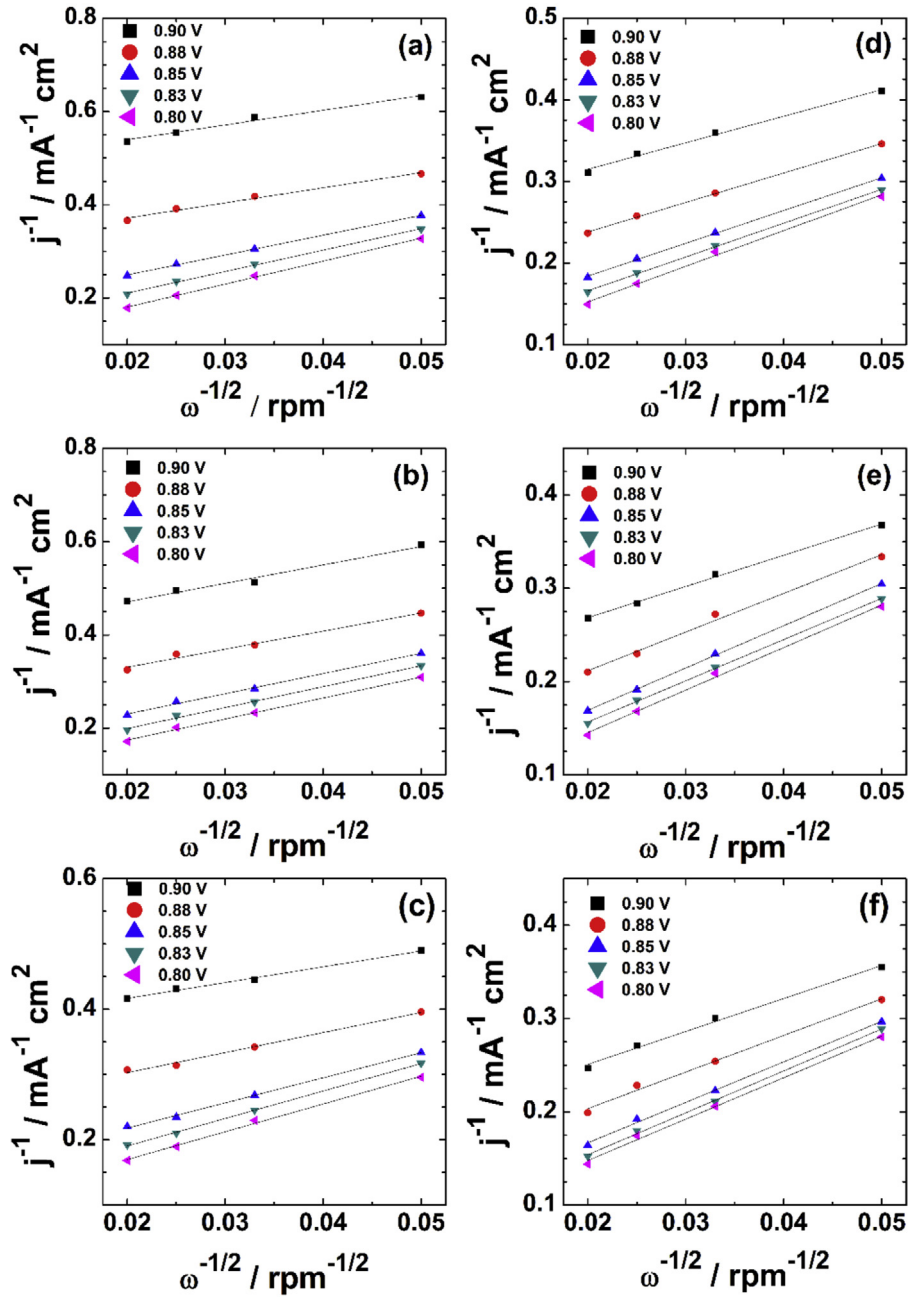
Fig. 5. RDE polarization curves of the Pt/C and PtCr/C electrocatalysts in a O_2-saturated 0.1 mol L^{-1} HClO$_4$ solution recorded at 1600 rpm, 5 mV s^{-1} and (a) 20 °C, (b) 30 °C, (c) 40 °C. Tafel plots of oxygen reduction reaction on Pt/C and PtCr/C in 0.1 mol L^{-1} HClO$_4$ recorded at 5 mV s^{-1} and (d) 20 °C, (e) 30 °C, (f) 40 °C for low current density (l.c.d) and high current density (h.c.d) region.

Table 2
The kinetic parameters deduced from the oxygen reduction polarization curves on Pt/C and Pt-Cr/C electrocatalysts in 0.1 mol L^{-1} HClO$_4$ at 20, 30 and 40 °C.

T/°C	Pt/C				Pt-Cr/C			
	20 °C	30 °C	40 °C	RRDE	20 °C	30 °C	40 °C	RRDE
n electron transfer number	4	4	4	4	4	4	4	4
$j_{k'}$ (mA cm^{-2})$^{@0.90V}$	0.042	0.044	0.043	0.065	0.045	0.037	0.050	0.081
j_L (mA cm^{-2})	110.37	142.85	124.30	129	126.05	139.64	120.71	112
b (mV/dec)$^{l.c.d}$/$^{h.c.d}$	68/114	86/162	90/124	66/116	70/128	83/137	68/124	73/118
j_o (mA cm^{-2})$^{l.c.d}$	9.32×10^{-4}	6.01×10^{-3}	5.04×10^{-3}	3.34×10^{-4}	1.89×10^{-3}	9.86×10^{-3}	4.76×10^{-3}	1.62×10^{-3}
j_o (mA cm^{-2})$^{h.c.d}$	4.92×10^{-2}	3.45×10^{-1}	4.55×10^{-2}	2.71×10^{-2}	1.62×10^{-1}	2.53×10^{-1}	8.60×10^{-2}	5.02×10^{-2}
p(H$_2$O)% $^{@0.90V}$	–	–	–	99.95	–	–	–	99.97
p(H$_2$O$_2$)%$^{@0.90V}$	–	–	–	0.05	–	–	–	0.03

Fig. 6. Koutecky-Levich plots (inverse of the current density j vs. inverse of the square root of rotation rate ω) of (a) Pt/C at 20 °C, (b) Pt/C at 30 °C, (c) Pt/C at 40 °C, (d) PtCr/C at 20 °C, (e) PtCr/C at 30 °C and (f) PtCr/C at 40 °C in 0.1 mol L^{-1} HClO$_4$.

tallographic structure. The negative 2θ shift observed in this case confirms this finding. The well-known Scherrer's equation as shown in Eq. (5) is used to extract basic data from the patterns like mean crystallite size (L).

$$L = \frac{k\lambda_{K\alpha}}{\beta \cos(\theta_B)} \tag{5}$$

where k is the Scherrer constant for the full width half maximum (FWHM) of spherical crystals of uniform size with cubic symmetry, $\lambda_{K\alpha}$ is the average value of wavelength of X-ray radiation, θ_B is the diffraction angle. β is commonly expressed as a FWHM (in radians) of the reflection (background subtracted) corrected for instrumental broadening and hkl is Miller indices. The lattice parameter is calculated by two methods: interplanar spacing of crystallographic
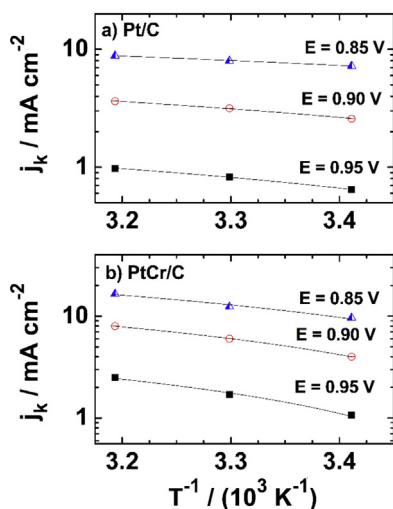
planes (hkl) method (in Eq. (7)) and Bragg's law in (Eq. (8)) which is made up of Eqs. (6) and (7). The findings are summarized in Table 1.

$$\lambda = 2d_{hkl}\sin(\theta) \tag{6}$$

$$\frac{1}{d_{hkl}^2} = \frac{(h^2 + k^2 + l^2)}{a_{hkl}^2} \tag{7}$$

$$\sin^2\theta = \frac{\lambda^2}{4a^2}(h^2 + k^2 + l^2) \tag{8}$$

The average crystallite size evaluated by using (220) planes for Pt/C and PtCr/C electrocatalysts is 6.68 nm and 3.43 nm, respectively. The average crystallite sizes estimated from XRD were slightly higher than the mean particle size values determined from TEM observations. The lattice parameter related to Pt/C is smaller than that of PtCr/C, confirming a progressive introduction of Cr into

Fig. 7. Electrochemical Arrhenius plots for the kinetic current densities of the oxygen reduction reaction on (a) Pt/C and (b) Pt-Cr/C recorded at different potentials in the temperature of 20 °C, 30 °C and 40 °C.

the alloyed state. The decrease in the Pt d-band vacancies may induce an increase in the lattice parameters hence larger Pt—Pt bond distance are formed as a result of alloying of Cr with Pt. However, Scherrer equation is inappropriate for the crystallites smaller than 3.0 nm. In fact, when the size is too small, phenomena like size effect and strain contributions strongly affect the broadening of the diffraction pattern [20,55].
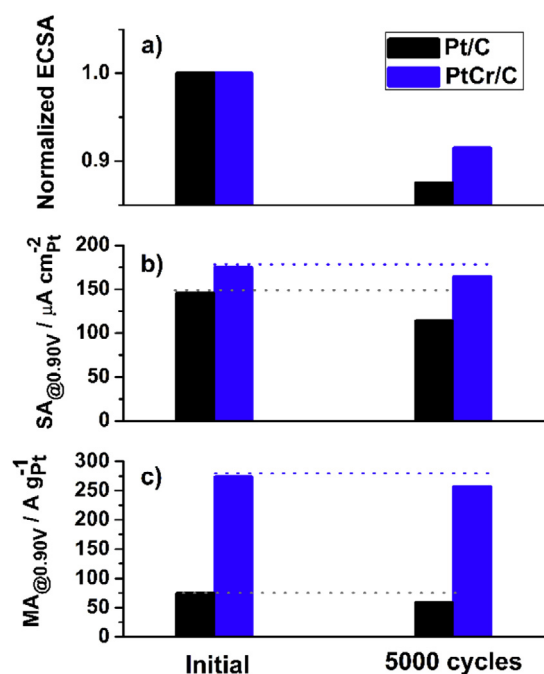
3.2. HRTEM of Pt/C and PtCr/C materials

Figs. 2 and 3 show that TEM micrographs and particle size distribution for the Pt/C and PtCr/C materials. The mean particle size ($D_{m.p}$) is evaluated by considering about 1000 isolated nanoparticles and fitting the histograms using a Log-Normal function. Both Pt/C and PtCr/C materials exhibit a well-dispersed and narrowly distributed nanoparticles with a small mean particle size, *ca.* 1.30 and 2.4 nm respectively.

While the platinum metal nanoparticles show up homogeneous distribution on the carbon substrate, the binary platinum-chromium materials show some inhomogeneities of nanoparticles with some agglomerates over the carbon support (Fig. 3).

3.3. Electrochemical characterization by cyclic voltammetry

Cyclic voltammetry (CV) provides qualitative information about electrochemical response of the materials with respect to some electrochemical reactions. It can be clearly seen in Fig. 4 that cyclic voltammograms of the Pt/C and PtCr/C electrodes are made of three characteristic potential regions (hydrogen region, double layer region and oxygen region) in oxygen free electrolyte recorded at 50 mV s^{-1} and 20, 30 and 40 °C. Hydrogen is adsorbed at the Pt surface during the backward potential scan and oxidized reversibly during the forward scan, giving rise to two pairs of peaks between 0.05 and 0.35 V *vs.* RHE at the hydrogen adsorption/desorption region. In the double layer region, between 0.35 and 0.65 V *vs.* RHE, no Faradaic reaction occurs and the capacitive current recorded results in the accumulation of charges from the electrolyte at the polarized interface. Oxygenated species start being chemisorbed, which leads to the formation of Pt hydroxide and oxide above 0.65 V *vs.* RHE and during the forward scan. The hydroxide/oxide species reduction current starts increasing during the backward scan to reach an optimum at *ca.* 0.70 V *vs.* RHE. The CV ends with another proton adsorption after the electrode surface became avail-
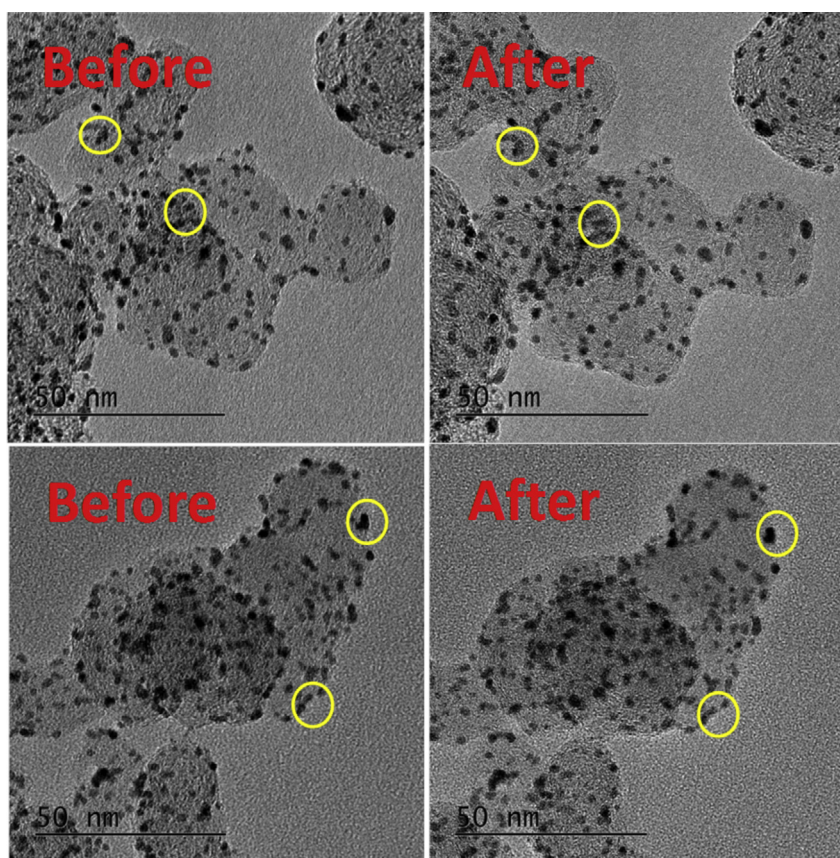

Fig. 8. Comparison of the a) normalized electrochemical surface area (ECSA) estimated by CO stripping coulometry b) ORR specific activity and c) ORR mass activity before and after an AST consisting of 5000 potential cycles between 0.60 and 1.00 V *vs.* RHE in 0.1 mol L^{-1} HClO$_4$. v = 0.050 V s^{-1}; T = 30 °C.

able passing through the double layer region. Compared to the CV of Pt/C, one observes in Fig. 4 that the oxygenated species are formed earlier at the PtCr/C surface during the forward scan and subsequently they start being reduced earlier (maximum at *ca.* 0.75 V *vs.* RHE) during the backward potential scan. The onset of anodic oxide film is directly related to the amount of free water available in the supporting electrolyte. As the activity of water used is the same, Pt-Cr bimetallic alloying causes the high onset potential of anodic oxide layer [56,57]. As can be seen in Fig. 4, the oxygen reduction peak on Pt/C is observed at 656.2, 665.7 and 678.1 mV *vs.* RHE with 3.8, 4.0, 4.3 mA cm^{-2} peak current densities recorded, respectively at 20, 30 and 40 °C, whereas those on Pt-Cr/C are at 689.7, 706.6 and 721.2 mV *vs.* RHE with 4.8, 5.1, 5.2 mA cm^{-2} peak current densities, respectively, in the same temperature range. This indicates that the weakly adsorbed oxide layer on the surface of Pt-Cr/C is easier to be reduced, and then increases the oxygen reduction activity [58,59]. Cyclic voltammetry features explicitly reveal that the incorporation of Cr results in a large electrochemically active surface area producing higher mass activity in Pt-Cr/C than Pt/C. It can thus be concluded that the bimetallic PtCr/C electrocatalysts have effective sites more energetically favorable than those of Pt/C in the oxidation/adsorption and reduction/desorption reactions [60,61].

3.4. Determination of the kinetic parameters from Koutecký-Levich equation

Fig. 5 displays RDE measurements related to the oxygen reduction reaction (ORR) activity of Pt/C and PtCr/C electrocatalysts as a function of the 1600 rpm recorded at 5 mV s^{-1} and different temperatures. It can be seen from that the onset potential of the ORR and the half-wave potential were significantly shifted to more positive potential values in the case of PtCr/C electrode, indicating its higher electrocatalytic activity compared to that of Pt/C. That is, the onset potential of the oxygen reduction reaction as regards Pt/C and PtCr/C electrocatalysts increases from 0.94 to reach 0.96 V *vs.* RHE when the temperature raises from 20 to 40 °C (Fig. 5a–c).

Fig. 9. Representative IL-TEM images of Pt/C catalysts before and after 5000 potential cycles between 0.60 and 1.00 V *vs.* RHE in 0.1 mol L^{-1} HClO$_4$. The yellow circles show the morphological changes of the electrocatalyst (crystallite migration and further aggregation and a low extend of particles detachment are highlighted). v = 0.050 V s^{-1}; T = 30 °C. (For interpretation of the references to colour in this figure legend, the reader is referred to the web version of this article.)

The experimental data of the ORR allow comparing the catalytic activity of the as-prepared electrode materials and its kinetic parameters from Koutecký-Levich equation (Eq. (9)) [62].

$$\frac{1}{|j|} = \frac{1}{|j_k|} + \frac{1}{|j_{d_L}|} \tag{9}$$

where j is the measured current density, j_k is the kinetic current density controlled by electron transfer kinetics, jd_L is the diffusion-limited current density of O$_2$ in the bulk electrolyte. The j_k term can be expressed as follows:

$$\frac{1}{|j_k|} = \frac{1}{|j_L|} + \frac{1}{|j_o|\left(\theta/\theta_e\right)\exp\left(\frac{|\eta|}{b}\right)} \tag{10}$$

where j_L is the diffusion-limiting current density as the key phenomenon of O$_2$ mass transport; it depends on the catalytic film thickness and less the adsorption contribution [63–65]. j_o represents the exchange current density, θ and θ_e are the coverage degrees of the electrode surface by oxygen containing adsorbed species at potential E and the equilibrium potential E_{eq} (E_{eq} = 1.186 V *vs.* RHE) [66], respectively. η is the overpotential (V) and b, the Tafel slope (mV dec^{-1}). Assuming that the adsorption process of oxygen is faster than the charge transfer step then $\theta \approx \theta_e$ at all the electrode potentials [18].

The diffusion limiting current density can be elucidated by Eq. (11).

$$|j_{d_L}| = 0.201nFD_{O_2}^{2/3}\omega^{1/2}\upsilon^{-1/6}C_{O_2}^* = B\omega^{1/2} \tag{11}$$

where B is the Levich slope, n is the number of transferred electrons per reduced oxygen molecule, F is the Faraday constant (96485 C mol^{-1}), D_{O_2} is the oxygen diffusion coefficient

(1.7 × 10^{-5} cm^2 s^{-1}), ω is the rotation rate of the electrode in revolution per minute. υ is the kinematic viscosity of the electrolyte (1.009 × 10^{-2} cm^2 s^{-1}) and $C_{O_2}^*$ is the oxygen concentration in the considered electrolyte (1.26 × 10^{-3} mol L^{-1}). The values of these coefficients are referred to a 0.1 mol L^{-1} HClO$_4$ solution, as reported [66–68]. Furthermore, the knowledge of the Levich constant (B) the number of the electrons exchanged (n$_e$) in the ORR can also be obtained according to Eq. (11) (Table 2).
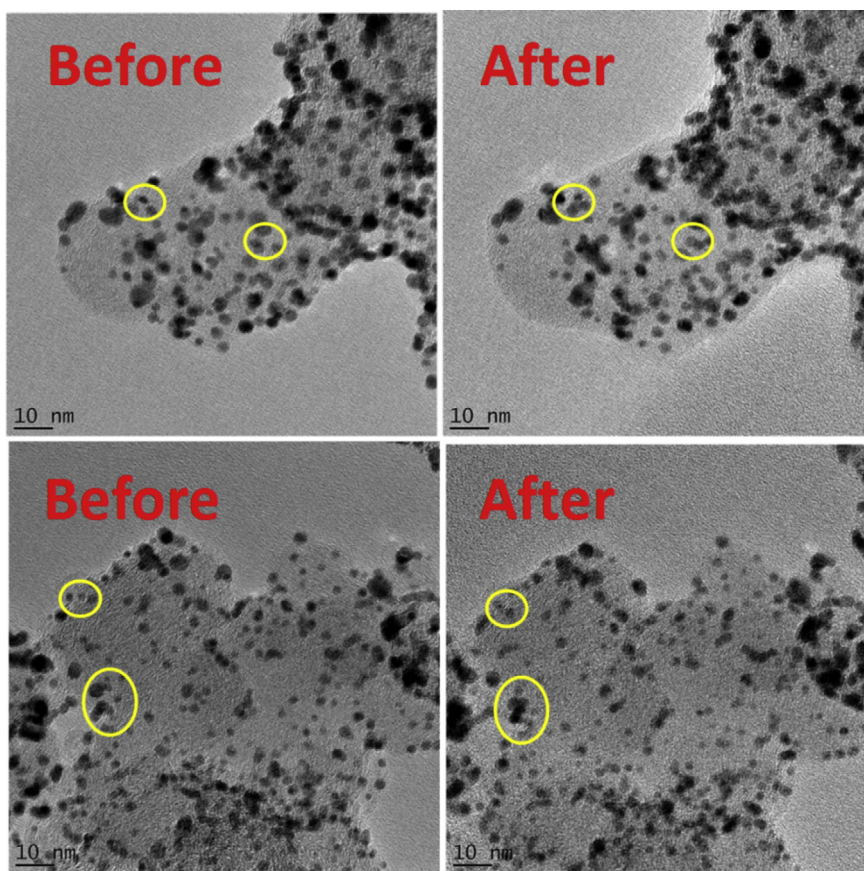
To evaluate the contribution of j_L, Koutecky-Levich plots were first obtained from j^{-1} as function of $\omega^{-1/2}$ for various electrode potentials around the half-wave one. As can be seen in Fig. 6, these plots are straight lines, indicating that the oxygen reduction reaction on the electrode surface is a first order process. Taking into account Eqs. (9) and (11) the corresponding j_k values can be easily estimated from the intercept; as the kinetic current density is free from mass transport, the specific current density $j_k^{'}$ value can be normalized with ECSA as expressed in Eq. (12).

$$j_k^{'}(mAcm^{-2}) = \frac{j_k(mAcm^{-2})}{SA(cm^{-2})}A_{geo}(cm^2) \tag{12}$$

where SA and A$_{geo}$ are the active surface area of the catalysts and the geometric surface area of the working electrode, respectively.

Tafel slope is one of the most frequently used diagnostic gauges in the clarification of the electrochemical reaction mechanisms dependency on temperature. After deducing j_L from the plot of $1/j_k$ as function of overpotential according to Eq. (10) (or E, since Eeq is

Fig. 10. Representative IL-TEM images of PtCr/C catalysts before and after 5000 potential cycles between 0.60 and 1.00 V *vs.* RHE in 0.1 mol L^{-1} HClO$_4$. The yellow circles show the morphological changes of the electrocatalyst (crystallite migration and further aggregation and a low extend of particles detachment are highlighted). v = 0.050 V s^{-1}; T = 30 °C. (For interpretation of the references to colour in this figure legend, the reader is referred to the web version of this article.)

a constant), Eq. (13) allows determining both the exchange current (j_0) and the Tafel slope, as expressed:

$$|\eta| = E - E_{eq} = -b \left[\ln \frac{j_L}{j_o} + \ln \frac{j_k}{j_L - j_k} \right] \qquad (13)$$
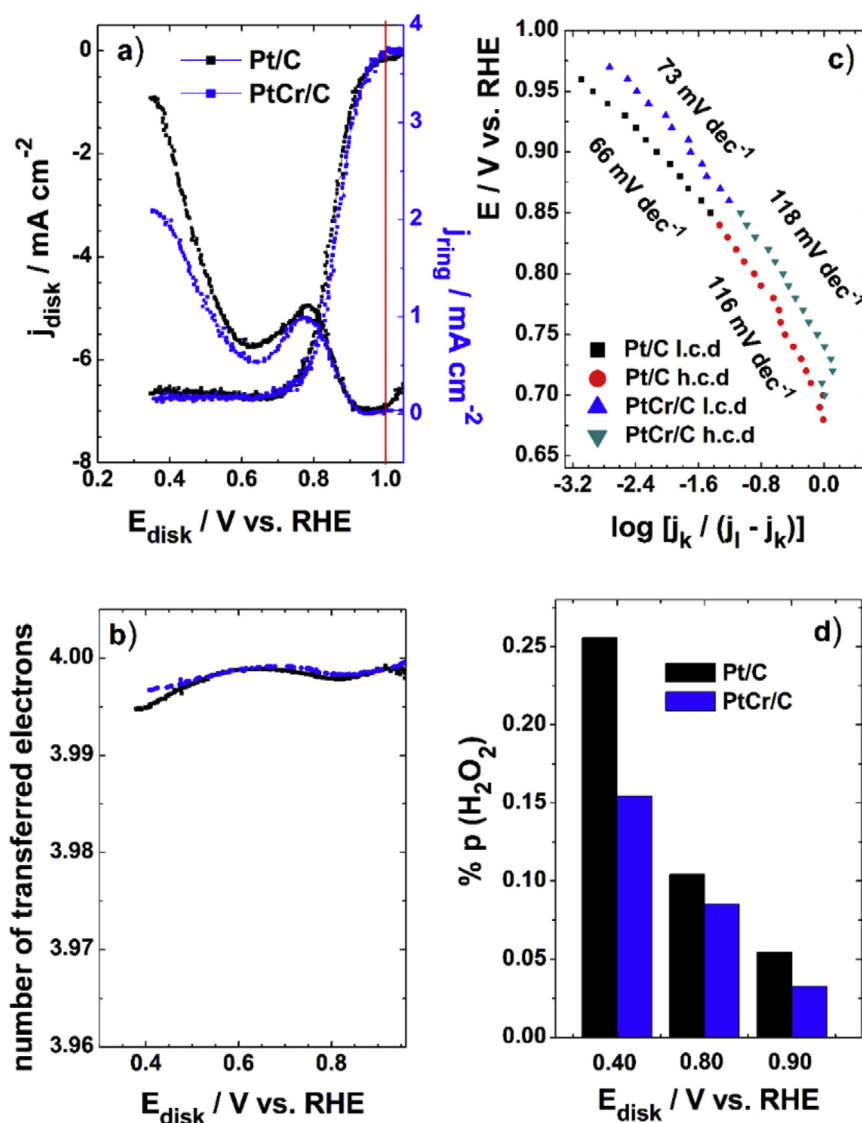
Each Tafel plot is essentially divided into two linear regions as referred to low current density region (l.c.d) and high current density region (h.c.d) with distinctly different slopes. These data are corrected for mass-transport effects by calculating the $j_k/(j_L - j_k)$. j_L is the limiting current density obtained from intercepts of the current density at disk electrode. The Tafel slopes in high current density (h.c.d) and low current density (l.c.d) regions shown in Fig. 5 are 68/114, 86/162, 90/124 mV dec^{-1} for Pt/C, and 70/128, 83/137, 68/124 mV dec^{-1} for Pt-Cr/C at the 20, 30 and 40 °C, respectively. These can be explained in terms of the different adsorption isotherms of oxygenated species, either Temkin isotherm has high coverage of surface oxides and/or adsorbed oxygen intermediates at low overpotential or Langmuir isotherm has low coverage of surface oxides and/or oxygen species at high overpotential [23]. Each of the Tafel plots in Fig. 5 was measured at four different RDE rotation rates ranging from 400 to 2500 rpm. The Tafel slope of -120 ± 10 mV dec^{-1} at the high current density region indicates that the enhancement in the oxygen reduction reaction catalytic activity at the Pt-Cr/C electrocatalyst is dominantly underwent the same reaction step as that of Pt/C electrocatalyst. However, by increasing the electrolyte temperature at *ca.* 30 °C, the Tafel plots are described by higher slopes. Thus, it can be concluded that orientation of the active sites are rearranged by the temperature effect, resulting in different oxygen adsorption force. Depending on the Tafel slopes, the exchange current density j$_0$ (mA cm^{-2}) being the

intrinsic catalytic activity of an electrochemical reaction is evaluated from the Koutecky-Levich plots [23,62,69]. The findings are summarized in Table 2.

The temperature effect on the kinetics of oxygen reduction was evaluated by using the Arrhenius equation in Eq. (14) [70].

$$\left[\frac{\partial (\log j_k)}{\partial \left(1/T \right)} \right]_E = -\frac{E_a^*}{2.303R} \qquad (14)$$

where E_a^* is the activation energy, R is the gas constant (8.314 J K^{-1} mol^{-1}), j_k is the kinetic current density and T is the temperature in Kelvin. The Arrhenius plots for three different potentials (E = 0.95, 0.90 V and 0.85 V *vs.* RHE) for the Pt/C and PtCr/C materials are shown in Fig. 7. From the slopes of the Arrhenius plots correspond to activation energies are 24 and 21 kJ mol^{-1} at 0.90 V for Pt/C and PtCr/C, respectively. The fact that the electrocatalytic reactions occur in the case of the most active surface with lowest activation energy. The activation energies from our study are in close agreement with the values reported for single crystalline [71] and polycrystalline platinum [72,73] as 20 and 25 kJ mol^{-1}, respectively. These calculated values were reported for the oxygen reduction reaction up to 50 kJ mol^{-1} in acid media [49,74–76]. The evaluation of the apparent activation energy at the 20, 30 and 40 °C indicates that apparent activation energy for oxygen reduction reaction is affected by temperature, *i.e.* more the temperature increases, and more the diffusion-controlled reaction is facilitated.

Fig. 11. Hydrodynamic voltammograms related to ORR for Pt/C and PtCr/C in a O_2-saturated 0.1 mol L^{-1} $HClO_4$ solution recorded at 5 mV s^{-1} and 1600 rpm. a) Ring electrode and disk electrode current density b) average number of transferred electrons c) Tafel plots for low current density (l.c.d) and high current density (h.c.d) regions and d) fraction of peroxide from the oxygen reduction reaction detected on the ring electrode at 0.90, 0.80 and 0.40 V vs. RHE.

3.5. Stability tests of the electrode materials

An accelerated stress test (AST) was performed to investigate and compare the stability trends of the Pt/C and the PtCr/C electrocatalysts. As mentioned in the experimental section, the aging procedure consisted of 5000 potential cycles between 0.60 and 1.00 V vs. RHE at a scan rate of 0.05 V s^{-1} in 0.1 mol L^{-1} $HClO_4$ and at 30 °C.

Fig. 8 shows the variations of the normalized electrochemically active surface area (ECSA), of the specific activity and of the mass activity for the ORR for the fresh/aged Pt/C and PtCr/C electrocatalysts. At the light of these results, PtCr/C appears to be more stable; only 8,5% of ECSA loss is monitored on the bimetallic catalyst against 12,5% for the Pt/C. In terms of both specific and mass activity, PtCr is also more robust. These results have however to be taken with caution because the stability enhancement reported in this study is not necessary due to the presence of Cr. It is well known that the ORR is a structure-sensitive reaction [77] and in that respect, the platinum particle size plays a major role. The lower particle size presents a larger fraction of low-coordinated sites on their surface, which strongly adsorb ORR intermediate thus impacting negatively the activity. Stability trends are also closely linked to particle size. As an example, Pt dissolution/redeposition mechanism is driven by dependence of the surface tension (and thus the redox potential) on the size of the crystallites. Having in mind that the PtCr/C particles are larger than the Pt/C, it is thus difficult to conclude on the origin of the robustness of PtCr/C compared to Pt/C.

To go further into the morphological changes of these two materials, an IL TEM study following the same AST was carried out; representative images before and after are shown in Figs. 9 and 10 for Pt/C and PtCr/C materials, respectively. In both cases, the changes are minor in agreement with the slight variations observed in Fig. 8. Among the nature of the degradation mechanism, one can report aggregation of neighbouring particles eventually followed by their coalescence. In some zones (particularly for the Pt/C catalyst), particles detachment has taken place. Here again, the particle size must be taken into account. The smaller particles are more prone to detach from the carbon support owing to their lower contact surface area with the carbon support.

3.6. RRDE measurements on the Pt-based electrocatalysts

Fig. 11 represents the polarization curves for the oxygen reduction reaction on Pt/C and PtCr/C, along with data on the corresponding formation of peroxide and number of transferred electrons. As the rotating ring disk electrode (RRDE) provides information on the intermediates of the oxygen reduction to H_2O, the amount of formation of peroxide and the number of involved electrons are calculated from Eqs. (15)–(18).

$$N = \frac{I_{Ring}}{I_{Disk}} \tag{15}$$

$$p(H_2O) = \frac{N|I_{disk}| - I_{ring}}{N|I_{disk}| + I_{ring}} \tag{16}$$

$$p(H_2O_2) = 1 - p(H_2O) \tag{17}$$

$$n = 4p(H_2O) + 2(1 - p(H_2O)) \tag{18}$$

where N is the collection efficiency, which is determined by ring current and disk current-potential curves recorded at $5\,mV\,s^{-1}$ in a N_2-deareated $0.1\,mol\,L^{-1}\,HClO_4 + 10\,mmol\,L^{-1}\,[Fe(III)(CN)6]^{3-}$ aqueous solution, $p(H_2O)$ is the fraction of water, $p(H_2O_2)$ is the fraction of peroxide and n, the number of exchanged electrons during the ORR. We clearly deduce from the half-wave potentials ($E_{1/2}$), which shifts about $16.40\,mV$ towards positive potential values (Fig. 11a) that the rate of O_2 reduction is enhanced on PtCr/C with the formation of low peroxide amounts. As can be seen in Fig. 11b, the determined number of exchanged electrons is close to 4.0 as a function of the disk electrode potential. The Tafel plots for the Pt/C and PtCr/C electrocatalysts are shown in Fig. 11c. Additionally, Fig. 11d summarizes the yield of H_2O_2 formation at 0.90, 0.80 and $0.40\,V$ vs. RHE. From an electrochemistry point of view, the enhanced reaction rate can be evidenced by the variation of the Tafel slope values depending on the oxygen-metal bond interaction. Pt/C and PtCr/C electrocatalysts are characterized by two different Tafel slopes $66/73\,mV\,dec^{-1}$ in low current density (Temkin isotherms) and $116/118\,mV\,dec^{-1}$ in high current density (Langmuir isotherms) regions. Within the fitting error, the Tafel slope does not find any dependency on the catalyst composition, their structure, supporting that the presence of the chromium does not involve changes in the ORR mechanism. As summarized in Table 2, the exchange current densities corresponding to each of the Tafel slopes are calculated to be $3.34 \times 10^{-4}/1.62 \times 10^{-3}$ and $2.71 \times 10^{-2}/5.02 \times 10^{-2}\,mA\,cm^{-2}$ [20,78] for Pt/C and PtCr/C, implying higher oxygen reduction activity on the PtCr/C electrocatalysts in comparison with the values reported [59,70,78–80].

4. Conclusions

Homogenously dispersed carbon supported Pt and PtCr nanomaterials were synthesized from an exclusively modified microwave-assisted polyol method. This preparation with diethylene glycol used as solvent and reducing agent showed well that the pH value at which the metal precursors are dissolved in this reaction environment is the critical parameter of controlling the nanoparticles formation. By combining physical and electrochemical characterizations, these investigations provided evidences that these Pt-based materials with particle diameter lower than 3 nm are efficient catalysts for the ORR. It was shown by AST and IL-TEM that the "dilution" of the Pt precious metal with a costly cheaper transition metal one (Cr) resulted in PtCr/C electrocatalysts more stable than Pt/C after 5000 potential cycles between 0.6 and 1 V vs. RHE. This enhancement in the catalytic activity of PtCr/C can likely be correlated with the ligand effect due to the alloying trend in the material composition. Accordingly, the weakly adsorbed oxide layer at the PtCr surface is easier to be reduced, which increases

the ORR reactivity at higher potentials. The RRDE experiments performed in a O_2-saturated $0.1\,mol\,L^{-1}\,HClO_4$ solution permitted to determine the kinetic parameters from Koutecký-Levich equation and Tafel plots. With exchanged electrons values close to 4, it can be assumed that the ORR proceeds mainly through a four-electron mechanism route at the surface of the prepared PtCr materials. Subsequently, at half-wave potential (0.9 V vs. RHE) 0.03% of hydrogen peroxide was only produced, indicating that the excellent ability of the obtained PtCr/C catalyst can be promisingly used as cathode material in a solid polymer electrolyte fuel cell.

References

[1] V. Viswanathan, H.A. Hansen, J. Rossmeisl, J.K. Nørskov, Universality in oxygen reduction electrocatalysis on metal surfaces, ACS Catal. 2 (2012) 1654–1660.
[2] T. Toda, H. Igarashi, H. Uchida, M. Watanabe, Enhancement of the electroreduction of oxygen on Pt alloys with Fe, Ni, and Co, J. Electrochem. Soc. 146 (1999) 3750–3756.
[3] L. Zhang, H. Li, J. Zhang, Kinetics of oxygen reduction reaction on three different Pt surfaces of Pt/C catalyst analyzed by rotating ring-disk electrode in acidic solution, J. Power Sources 255 (2014) 242–250.
[4] M.K. Debe, Electrocatalyst approaches and challenges for automotive fuel cells, Nature 486 (2012) 43–51.
[5] K. Ke, T. Hatanaka, Y. Morimoto, Reconsideration of the quantitative characterization of the reaction intermediate on electrocatalysts by a rotating ring-disk electrode: the intrinsic yield of H2O2 on Pt/C, Electrochim. Acta 56 (2011) 2098–2104.
[6] J.K. Nørskov, J. Rossmeisl, A. Logadottir, L. Lindqvist, J.R. Kitchin, T. Bligaard, H. Jónsson, Origin of the overpotential for oxygen reduction at a fuel-cell cathode, J. Phys. Chem. B 108 (2004) 17886–17892.
[7] S. Mukerjee, S. Srinivasan, M.P. Soriaga, J. McBreen, Role of structural and electronic properties of Pt and Pt alloys on electrocatalysis of oxygen reduction: an in situ XANES and EXAFS investigation, J. Electrochem. Soc. 142 (1995) 1409–1422.
[8] V. Jalan, E.J. Taylor, Importance of interatomic spacing in catalytic reduction of oxygen in phosphoric acid, J. Electrochem. Soc. 130 (1983) 2299–2302.
[9] A. Damjanovic, M.A. Genshaw, J.O. Bockris, M. apos, Distinction between intermediates produced in main and side electrodic reactions, J. Chem. Phys. 45 (1966) 4057–4059.
[10] H.S. Wroblowa, P. Yen Chi, G. Razumney, Electroreduction of oxygen: a new mechanistic criterion, J. Electroanal. Chem. Interfacial Electrochem. 69 (1976) 195–201.
[11] A.J. Appleby, M. Savy, Kinetics of oxygen reduction reactions involving catalytic decomposition of hydrogen peroxide: application to porous and rotating ring-disk electrodes, J. Electroanal. Chem. Interfacial Electrochem. 92 (1978) 15–30.
[12] N.A. Anastasijević, V. Vesović, R.R. Adžić, Determination of the kinetic parameters of the oxygen reduction reaction using the rotating ring-disk electrode: part I. Theory, J. Electroanal. Chem. Interfacial Electrochem. 229 (1987) 305–316.
[13] R.W. Zurilla, R.K. Sen, E. Yeager, The kinetics of the oxygen reduction reaction on gold in alkaline solution, J. Electrochem. Soc. 125 (1978) 1103–1109.
[14] I. Katsounaros, W.B. Schneider, J.C. Meier, U. Benedikt, P.U. Biedermann, A.A. Auer, K.J. Mayrhofer, Hydrogen peroxide electrochemistry on platinum: towards understanding the oxygen reduction reaction mechanism, Phys. Chem. Chem. Phys. 14 (2012) 7384–7391.
[15] R. Jiang, S. Dong, Rotating ring disk electrode (RRDE) theory dealing with nonstationary electrocatalysis: study of the electrocatalytic reduction of dioxygen at cobalt protoporphin modified electrode, J. Phys. Chem. 94 (1990) 7471–7476.
[16] S. Walch, A. Dhanda, M. Aryanpour, H. Pitsch, Mechanism of molecular oxygen reduction at the cathode of a PEM fuel cell: non-electrochemical reactions on catalytic Pt particles, J. Phys. Chem. C 112 (2008) 8464–8475.
[17] E. Yeager, Electrocatalysts for O2 reduction, Electrochim. Acta 29 (1984) 1527–1537.
[18] E. Lebègue, S. Baranton, C. Coutanceau, Polyol synthesis of nanosized Pt/C electrocatalysts assisted by pulse microwave activation, J. Power Sources 196 (2011) 920–927.
[19] S. Song, Y. Wang, P.K. Shen, Pulse-microwave assisted polyol synthesis of highly dispersed high loading Pt/C electrocatalyst for oxygen reduction reaction, J. Power Sources 170 (2007) 46–49.

[20] Y. Holade, N.E. Sahin, K. Servat, T. Napporn, K. Kokoh, Recent advances in carbon supported metal nanoparticles preparation for oxygen reduction reaction in low temperature fuel cells, Catalysts 5 (2015) 310–348.

[21] F. Taufany, C.-J. Pan, H.-L. Chou, J. Rick, Y.-S. Chen, D.-G. Liu, J.-F. Lee, M.-T. Tang, B.-J. Hwang, Relating structural aspects of bimetallic Pt3Cr1/C nanoparticles to their electrocatalytic activity, stability, and selectivity in the oxygen reduction reaction, Chem.–Eur. J. 17 (2011) 10724–10735.

[22] J.M. Léger, Preparation and activity of mono- or bi-metallic nanoparticles for electrocatalytic reactions, Electrochim. Acta 50 (2005) 3123–3129.

[23] S. Beyhan, N.E. Şahin, S. Pronier, J.-M. Léger, F. Kadırgan, Comparison of oxygen reduction reaction on Pt/C, Pt-Sn/C, Pt-Ni/C, and Pt-Sn-Ni/C catalysts prepared by Bönnemann method: a rotating ring disk electrode study, Electrochim. Acta 151 (2015) 565–573.

[24] H. Noguchi, T. Okada, K. Uosaki, Molecular structure at electrode/electrolyte solution interfaces related to electrocatalysis, Faraday Discuss. 140 (2009) 125.

[25] D.V. Tripkovic, D. Strmcnik, D. van der Vliet, V. Stamenkovic, N.M. Markovic, The role of anions in surface electrochemistry, Faraday Discuss. 140 (2009) 25–40.

[26] A. Chen, P. Holt-Hindle, Platinum-based nanostructured materials: synthesis, properties, and applications, Chem. Rev. 110 (2010) 3767–3804.

[27] F. Somodi, Z. Peng, A.B. Getsoian, A.T. Bell, Effects of the synthesis parameters on the size and composition of Pt–Sn nanoparticles prepared by the polyalcohol reduction method, J. Phys. Chem. C 115 (2011) 19084–19090.

[28] A.R. Tao, S. Habas, P. Yang, Shape control of colloidal metal nanocrystals, Small 4 (2008) 310–325.

[29] T. Herricks, J. Chen, Y. Xia, Polyol synthesis of platinum nanoparticles: control of morphology with sodium nitrate, Nano Lett. 4 (2004) 2367–2371.

[30] L. Dubau, T. Asset, R. Chattot, C. Bonnaud, V. Vanpeene, J. Nelayah, F. Maillard, Tuning the performance and the stability of porous hollow PtNi/C nanostructures for the oxygen reduction reaction, ACS Catal. 5 (2015) 5333–5341.

[31] A. Anastasopoulos, J.C. Davies, L. Hannah, B.E. Hayden, C.E. Lee, C. Milhano, C. Mormiche, L. Offin, The particle size dependence of the oxygen reduction reaction for carbon-supported platinum and palladium, ChemSusChem 6 (2013) 1973–1982.

[32] K.J. Carroll, J.U. Reveles, M.D. Shultz, S.N. Khanna, E.E. Carpenter, Preparation of elemental Cu and Ni nanoparticles by the polyol method: an experimental and theoretical approach, J. Phys. Chem. C 115 (2011) 2656–2664.

[33] R.J. Joseyphus, T. Matsumoto, H. Takahashi, D. Kodama, K. Tohji, B. Jeyadevan, Designed synthesis of cobalt and its alloys by polyol process, J. Solid State Chem. 180 (2007) 3008–3018.

[34] L. Gan, H. Du, B. Li, F. Kang, Influence of reaction temperature on the particle-composition distributions and activities of polyol-synthesized Pt-Ru/C catalysts for methanol oxidation, J. Power Sources 191 (2009) 233–239.

[35] J. Ungelenk, M. Speldrich, R. Dronskowski, C. Feldmann, Polyol-mediated low-temperature synthesis of crystalline tungstate nanoparticles MWO4 (M = Mn, Fe Co, Ni, Cu, Zn), Solid State Sci. 31 (2014) 62–69.

[36] J.A. Gerbec, D. Magana, A. Washington, G.F. Strouse, Microwave–enhanced reaction rates for nanoparticle synthesis, J. Am. Chem. Soc. 127 (2005) 15791–15800.

[37] M. Tsuji, M. Hashimoto, Y. Nishizawa, M. Kubokawa, T. Tsuji, Microwave–assisted synthesis of metallic nanostructures in solution, Chem.–Eur. J. 11 (2005) 440–452.

[38] H. Kawasaki, Y. Kosaka, Y. Myoujin, T. Narushima, T. Yonezawa, R. Arakawa, Microwave–assisted polyol synthesis of copper nanocrystals without using additional protective agents, Chem. Commun. 47 (2011) 7740–7742.

[39] B.G. Pollet, Let's not ignore the ultrasonic effects on the preparation of fuel cell materials, Electrocatalysis 5 (2014) 330–343.

[40] H. Tong, H.-L. Li, X.-G. Zhang, Ultrasonic synthesis of highly dispersed Pt nanoparticles supported on MWCNTs and their electrocatalytic activity towards methanol oxidation, Carbon 45 (2007) 2424–2432.

[41] H. Yano, M. Kataoka, H. Yamashita, H. Uchida, M. Watanabe, Oxygen reduction activity of carbon-supported Pt-M (M = V, Ni, Cr, Co, and Fe) alloys prepared by nanocapsule method, Langmuir 23 (2007) 6438–6445.

[42] S. Chen, W. Sheng, N. Yabuuchi, P.J. Ferreira, L.F. Allard, Y. Shao-Horn, Origin of oxygen reduction reaction activity on Pt3Co nanoparticles: atomically resolved chemical compositions and structures, J. Phys. Chem. C 113 (2008) 1109–1125.

[43] C. Venkateswara Rao, B. Viswanathan, ORR activity and direct ethanol fuel cell performance of carbon-Supported Pt-M (M = Fe, Co, and Cr) alloys prepared by polyol reduction method, J. Phys. Chem. C 113 (2009) 18907–18913.

[44] M. Huang, L. Li, Y. Guo, Microwave heated polyol synthesis of Pt3Te/C catalysts, Electrochim. Acta 54 (2009) 3303–3308.

[45] F. Colmati, E. Antolini, E.R. Gonzalez, Pt–Sn/C electrocatalysts for methanol oxidation synthesized by reduction with formic acid, Electrochim. Acta 50 (2005) 5496–5503.

[46] R.-F. Wang, S.-J. Liao, H.-Y. Liu, H. Meng, Synthesis and characterization of Pt-Se/C electrocatalyst for oxygen reduction and its tolerance to methanol, J. Power Sources 171 (2007) 471–476.

[47] Y.-H. Cho, O.-H. Kim, D.Y. Chung, H. Choe, Y.-H. Cho, Y.-E. Sung, PtPdCo ternary electrocatalyst for methanol tolerant oxygen reduction reaction in direct methanol fuel cell, Appl. Catal. B: Environ. 154–155 (2014) 309–315.

[48] Y. Zhou, D. Zhang, Nano PtCu binary and PtCuAg ternary alloy catalysts for oxygen reduction reaction in proton exchange membrane fuel cells, J. Power Sources 278 (2015) 396–403.

[49] M.K. Jeon, Y. Zhang, P.J. McGinn, A comparative study of PtCo, PtCr, and PtCoCr catalysts for oxygen electro-reduction reaction, Electrochim. Acta 55 (2010) 5318–5325.

[50] E. Antolini, J.R.C. Salgado, L.G.R.A. Santos, G. Garcia, E.A. Ticianelli, E. Pastor, E.R. Gonzalez, Carbon supported Pt–Cr alloys as oxygen-reduction catalysts for direct methanol fuel cells, J. Appl. Electrochem. 36 (2006) 355–362.

[51] H. Yang, N. Alonso-Vante, C. Lamy, D.L. Akins, High methanol tolerance of carbon-supported Pt-Cr alloy nanoparticle electrocatalysts for oxygen reduction, J. Electrochem. Soc. 152 (2005) A704–A709.

[52] M.C. Escaño, E. Gyenge, H. Nakanishi, H. Kasai, Pt/Cr and Pt/Ni catalysts for oxygen reduction reaction: to alloy or not to alloy? J. Nanosci. Nanotechnol. 11 (2011) 2944–2951.

[53] H. Yang, N. Alonso-Vante, J.-M. Léger, C. Lamy, Tailoring, structure, and activity of carbon-supported nanosized Pt-Cr alloy electrocatalysts for oxygen reduction in pure and methanol-containing electrolytes, J. Phys. Chem. B 108 (2004) 1938–1947.

[54] R.C. Koffi, C. Coutanceau, E. Garnier, J.M. Léger, C. Lamy, Synthesis, characterization and electrocatalytic behaviour of non-alloyed PtCr methanol tolerant nanoelectrocatalysts for the oxygen reduction reaction (ORR), Electrochim. Acta 50 (2005) 4117–4127.

[55] L.A. Estudillo-Wong, Y. Luo, J.A. Díaz-Real, N. Alonso-Vante, Enhanced oxygen reduction reaction stability on platinum nanoparticles photo-deposited onto oxide-carbon composites, Appl. Catal. B: Environ. 187 (2016) 291–300.

[56] K.J.J. Mayrhofer, B.B. Blizanac, M. Arenz, V.R. Stamenkovic, P.N. Ross, N.M. Markovic, The impact of geometric and surface electronic properties of Pt-catalysts on the particle size effect in electrocatalysis, J. Phys. Chem. B 109 (2005) 14433–14440.

[57] D. Chen, Q. Tao, L.W. Liao, S.X. Liu, Y.X. Chen, S. Ye, Determining the active surface area for various platinum electrodes, Electrocatalysis 2 (2011) 207–219.

[58] C.S. Rao, D.M. Singh, R. Sekhar, J. Rangarajan, Pt–Co electrocatalyst with varying atomic percentage of transition metal, Int. J. Hydrogen Energy 36 (2011) 14805–14814.

[59] L.G.R.A. Santos, C.H.F. Oliveira, I.R. Moraes, E.A. Ticianelli, Oxygen reduction reaction in acid medium on Pt–Ni/C prepared by a microemulsion method, J. Electroanal. Chem. 596 (2006) 141–148.

[60] J.B. Floriano, E.A. Ticianelli, E.R. Gonzalez, Influence of the supporting electrolyte on the oxygen reduction reaction at the platinum/proton exchange membrane interface, J. Electroanal. Chem. 367 (1994) 157–164.

[61] K.J.J. Mayrhofer, D. Strmcnik, B.B. Blizanac, V. Stamenkovic, M. Arenz, N.M. Markovic, Measurement of oxygen reduction activities via the rotating disc electrode method: from Pt model surfaces to carbon-supported high surface area catalysts, Electrochim. Acta 53 (2008) 3181–3188.

[62] C. Coutanceau, M.J. Croissant, T. Napporn, C. Lamy, Electrocatalytic reduction of dioxygen at platinum particles dispersed in a polyaniline film, Electrochim. Acta 46 (2000) 579–588.

[63] S.K. Zecevic, J.S. Wainright, M.H. Litt, S.L. Gojkovic, R.F. Savinell, Kinetics of O2 reduction on a Pt electrode covered with a thin film of solid polymer electrolyte, J. Electrochem. Soc. 144 (1997) 2973–2982.

[64] S.L. Gojković, S.K. Zečević, R.F. Savinell, O2 reduction on an ink-Type rotating disk electrode using Pt supported on high-area carbons, J. Electrochem. Soc. 145 (1998) 3713–3720.

[65] F. Gloaguen, F. Andolfatto, R. Durand, P. Ozil, Kinetic study of electrochemical reactions at catalyst-recast ionomer interfaces from thin active layer modelling, J. Appl. Electrochem. 24 (1994) 863–869.

[66] K.E. Gubbins, R.D. Walker, The solubility and diffusivity of oxygen in electrolytic solutions, J. Electrochem. Soc. 112 (1965) 469–471.

[67] C. Grolleau, C. Coutanceau, F. Pierre, J.M. Léger, Effect of potential cycling on structure and activity of Pt nanoparticles dispersed on different carbon supports, Electrochim. Acta 53 (2008) 7157–7165.

[68] N.M. Marković, H.A. Gasteiger, B.N. Grgur, P.N. Ross, Oxygen reduction reaction on Pt(111): effects of bromide, J. Electroanal. Chem. 467 (1999) 157–163.

[69] D. Diabaté, T.W. Napporn, K. Servat, A. Habrioux, S. Arrii-Clacens, A. Trokourey, K.B. Kokoh, Kinetic study of oxygen reduction reaction on carbon supported Pd-based nanomaterials in alkaline medium, J. Electrochem. Soc. 160 (2013) H302–H308.

[70] U.A. Paulus, A. Wokaun, G.G. Scherer, T.J. Schmidt, V. Stamenkovic, V. Radmilovic, N.M. Markovic, P.N. Ross, Oxygen reduction on carbon-Supported Pt-Ni and Pt-Co alloy catalysts, J. Phys. Chem. B 106 (2002) 4181–4191.

[71] B.N. Grgur, N.M. Marković, P.N. Ross, Temperature-dependent oxygen electrochemistry on platinum low-index single crystal surfaces in acid solutions, Can. J. Chem. 75 (1997) 1465–1471.

[72] A. Damjanovic, D.B. Sepa, An analysis of the pH dependence of enthalpies and Gibbs energies of activation for O2 reduction at Pt electrodes in acid solutions, Electrochim. Acta 35 (1990) 1157–1162.

[73] D.B. Sepa, M.V. Vojnovic, L.M. Vracar, A. Damjanovic, Apparent enthalpies of activation of electrodic oxygen reduction at platinum in different current density regions—I. Acid solution, Electrochim. Acta 31 (1986) 91–96.

[74] O. Solorza-Feria, S. Durón, Temperature effects for oxygen reduction on Ru-nanoparticles in acid solution, Int. J. Hydrogen Energy 27 (2002) 451–455.

[75] N.M. Marković, B.N. Grgur, P.N. Ross, Temperature-dependent hydrogen electrochemistry on platinum low-index single-crystal surfaces in acid solutions, J. Phys. Chem. B 101 (1997) 5405–5413.

[76] N. Wakabayashi, M. Takeichi, M. Itagaki, H. Uchida, M. Watanabe, Temperature-dependence of oxygen reduction activity at a platinum electrode in an acidic electrolyte solution investigated with a channel flow double electrode, J. Electroanal. Chem. 574 (2005) 339–346.

[77] F. Maillard, M. Martin, F. Gloaguen, J.M. Léger, Oxygen electroreduction on carbon-supported platinum catalysts. Particle-size effect on the tolerance to methanol competition, Electrochim. Acta 47 (2002) 3431–3440.

[78] J.X. Wang, N.M. Markovic, R.R. Adzic, Kinetic analysis of oxygen reduction on Pt(111) in acid solutions: intrinsic kinetic parameters and anion adsorption effects, J. Phys. Chem. B 108 (2004) 4127–4133.

[79] N. Wakabayashi, M. Takeichi, H. Uchida, M. Watanabe, Temperature dependence of oxygen reduction activity at Pt-Fe, Pt-Co, and Pt-Ni alloy electrodes, J. Phys. Chem. B 109 (2005) 5836–5841.

[80] U.A. Paulus, T.J. Schmidt, H.A. Gasteiger, R.J. Behm, Oxygen reduction on a high-surface area Pt/Vulcan carbon catalyst: a thin-film rotating ring-disk electrode study, J. Electroanal. Chem. 495 (2001) 134–145.